

# Static Hand Gesture Recognition for American Sign Language using Neuromorphic Hardware

MohammedReza Mohammadi<sup>1</sup>, Peyton Chandarana<sup>1</sup>, James Seekings, Sara Hendrix, Ramtin Zand

University of South Carolina, Columbia, SC 29201

E-mail: [ramtin@cse.sc.edu](mailto:ramtin@cse.sc.edu)

27 July 2022

<sup>1</sup>Authors contributed equally.

**Abstract.** In this paper, we develop four spiking neural network (SNN) models for two static American Sign Language (ASL) hand gesture classification tasks, i.e., the ASL Alphabet and ASL Digits. The SNN models are deployed on Intel’s neuromorphic platform, Loihi, and then compared against equivalent deep neural network (DNN) models deployed on an edge computing device, the Intel Neural Compute Stick 2 (NCS2). We perform a comprehensive comparison between the two systems in terms of accuracy, latency, power consumption, and energy. The best DNN model achieves an accuracy of 99.6% on the ASL Alphabet dataset, whereas the best performing SNN model has an accuracy of 99.44%. For the ASL-Digits dataset, the best SNN model outperforms all of its DNN counterparts with 99.52% accuracy. Moreover, our obtained experimental results show that the Loihi neuromorphic hardware implementations achieve up to  $14.67\times$  and  $4.09\times$  reduction in power consumption and energy, respectively, when compared to NCS2.

## 1. Introduction

Sign language is a visual language that enables people who are deaf or hard of hearing to communicate with others in their communities. To convey emotion, grammar, and sentence structure similar to spoken language, sign language employs visual and manual elements such as hand gestures, facial expressions, and body movements. Hand gestures are regarded as the fundamental component of a sign language vocabulary. In addition to these gestures, facial expressions and body movement are used to accentuate the emotions of words and phrases [1]. Hand gestures in a sign language can be classified as static or dynamic depending on whether or not hand motion is incorporated into the sign interpretations [2,3]. Static hand gestures, also known as static hand postures, consist of the shape and orientation of the hand and fingers and is commonly used for finger spelling alphabet letters and digits. Dynamic hand gestures, on the other hand, are a set of hand gestures with accompanied motion for word interpretation and translation.

Automatic hand gesture recognition is applicable to a variety of applications and has been a broad and significant research area over the last decade [4]. The most widely researched approaches to automatic hand gesture recognition employ motion sensors and vision sensors.

Motion sensor techniques collect and track hand gestures, finger orientation, and hand velocity using a range of sensors such as sensor gloves [5], motion controllers [6], accelerometers [7], magnetometers, and gyroscopes [8, 9]. The motion sensor-based approaches have the benefit of being able to accurately capture motion data in real-time. However, these sensors are typically expensive and inconvenient for signers since installing or wearing these instruments can restrict motion and thus hinder performance. Employing multiple motion sensors in a recognition system allows for a more precise recognition in particular sign language vocabularies but consequentially results in higher implementation cost and complexity. Many works in the past have therefore adopted multiple motion sensors simultaneously to increase classification accuracy of the performed signs [10–12].

On the other hand, vision-based approaches utilize at least one camera and image processing algorithms including segmentation, shape detection, motion tracking, color detection, and contour modeling to capture and recognize actual hand gestures without the need of cumbersome physical devices [13–16]. Since these approaches do not require wearing the devices to track motion, they are more user-friendly and comfortable without impeding the wearer’s motions. Similar to many other object detection and recognition applications, deep learning methods, particularly convolutional neural networks (CNNs), have recently become the primary choice for sign language applications [17–20]. However, the major downside of deep learning-based techniques is they often consume a significant amount of power [21]. Since hand gesture recognition models are typically intended to be deployed in portable devices like smartphones, tablets, and wearable devices like smart glasses, power and energy are major constraints. Low-power machine learning is an important field of study that can enable such applications at the edge devices. In particular, neuromorphic algorithms and hardware, which are inspired by the low-power processing of the human brain, have been attracting more attention in recent years [22, 23].

In 2018, Intel introduced a neuromorphic processor called Loihi capable of running spiking neural networks (SNNs) with orders of magnitude lower power consumption while achieving accuracies close to state-of-the-art CPU, GPU, and TPU implementations [24]. Along with Loihi, Intel provided a python library, NxSDK, for SNN design and deployment. NxSDK included many features for designing SNNs from scratch including setting learning rules for synaptic plasticity learning methods. This design methodology, however, does introduce its own complexities in design, training, and hyper-parameter tuning to get accurate and meaningful results.

While there are inherently many differences between how artificial neural networks (ANNs) and SNNs are trained and operate, conversion processes have been widely researched to convert ANNs to SNNs to reduce the complexity of the end-to-end design

of SNNs. In 2017, Rueckauer et. al. [25] developed the SNN Conversion Toolbox which aimed to convert trained ANN models to SNNs. While the concept of converting ANNs to SNNs was not novel at the time with many works introducing different conversion methods [26, 27], the SNN Conversion Toolbox intended to streamline the process for conversion by both creating a more automatic conversion pipeline and also implementing several features missing in the previous conversion works. Unlike previous conversion methods, the SNN Conversion Toolbox allows an ANN to be trained in a deep learning library like TensorFlow [28], PyTorch [29], or etc. with layers commonly found in CNN architectures. The toolbox implements spiking layers like average pooling and convolutional layers to provide a means for the models to be parsed and converted to SNNs without as much hyper-parameter tuning and design considerations. In 2021, Rueckauer et. al. [30] introduced NxTF which extended the SNN Conversion Toolbox to enable deployment of converted SNNs to Intel’s Loihi neuromorphic chip. NxTF was designed specifically to map layers found in the ANN models to layers which Loihi could understand through a custom NxSDK backend [23].

In this paper, we focus on classifying static images of the ASL Alphabet and ASL Digits. The following are our contributions:

- We design four ANN models and train each model with the ASL Alphabet and ASL Digit static image datasets for a total of eight models. We then convert them to SNNs using the SNN Conversion Toolbox.
- We analyze the trade-off between accuracy and latency and compare the differences when favoring accuracy or latency.
- We investigate methods for accurately measuring power and energy consumption.
- We compare and analyze the hardware performance of the ANN models on the Intel Neural Compute Stick 2 to the SNN models on Intel Loihi in terms of accuracy, latency, power consumption, and energy.

The subsequent sections of this paper are organized as follow. The datasets for this study are presented in Section 2. Section 3 describes the ANN model design. Section 4 provides a summarized background on the SNN Conversion Toolbox’s conversion methodology. Section 5 introduces the experimental methodology performed in this work including the processes for hardware deployment and measuring latency, power, and energy. The results of the experiments are discussed and evaluated in Section 6. Section 7 contains the conclusion and suggestions for future study.

## **2. ASL Datasets**

In this paper two different static image datasets are studied. The American Sign Language (ASL) Alphabet [31] is the first dataset which replaces the common handwritten digit dataset, MNIST [33], commonly used as an ANN model’s proof-of-concept classification test. The ASL Alphabet dataset includes static images of multiple people repeating ASL finger-spelling against various backdrops. With the exception

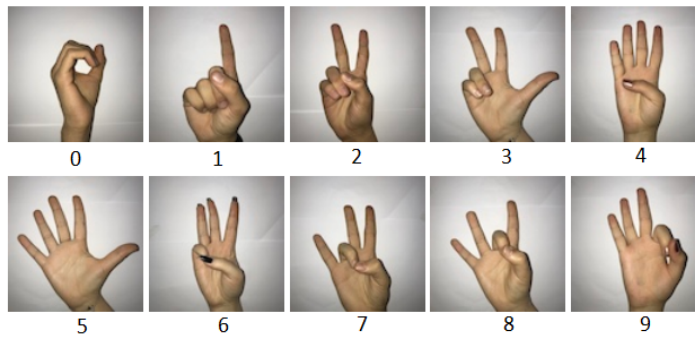
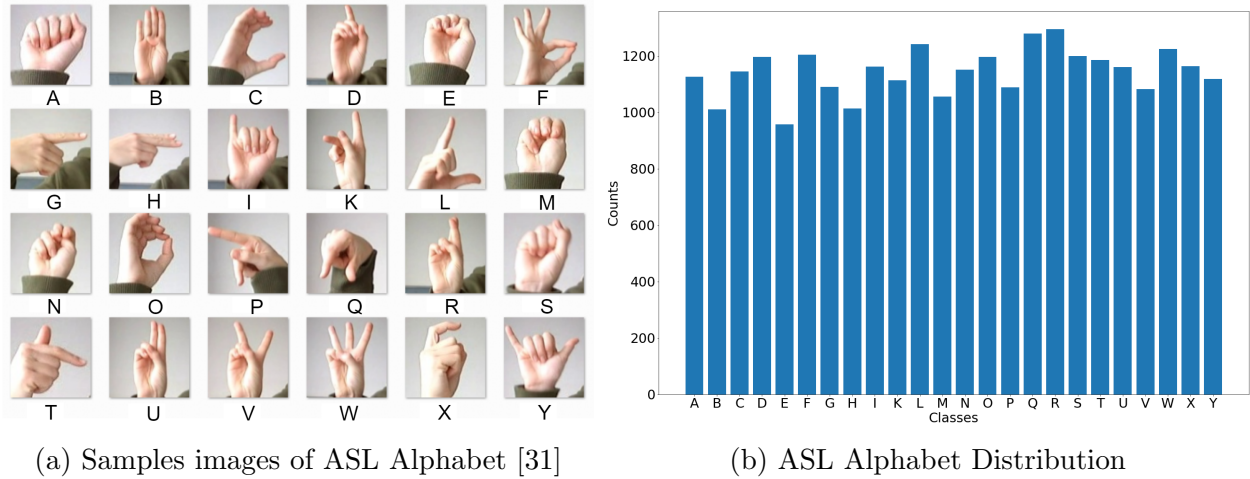


Figure 1: Samples of the ASL images used in classification. ASL Digits dataset has equal class distribution while the ASL Alphabet does not.

of J and Z, which require motion, the ASL Alphabet dataset of hand gestures is a multi-class problem with 24 classes of letters. Figure 1(a) depicts examples of each class. The ASL Alphabet, created by [31], dataset was constructed by considerably expanding a small set of color images, 1704 images, that were not cropped around the hand region of interest. The designers of the dataset, [31], generate additional data using an image processing pipeline which is comprised of cropping the images around the hands, converting the images to gray-scale, resizing the images, and then making more than 50 variations to increase the dataset size. Furthermore, the data augmentation includes the use of Mitchell, Hermite, and Catrom filters, coupled with 5% random noise,  $\pm 15\%$  brightness/contrast, and 3 degrees of image rotation. After these data augmentation steps, the dataset includes 34,627 gray-scale images of size  $28 \times 28$  pixels which are split into separate train, validation, and test datasets. 27,455 samples,  $\sim 80\%$ , of the ASL alphabet are used for training and validation, and 7,172 samples,  $\sim 20\%$ , are used for testing. Figure 1(b) shows the distribution of training samples across 24 classes.

The other dataset we employ in this study is the ASL Digits dataset [32]. It is

made up of 2062 RGB images with  $100 \times 100$  pixels that are divided into 10 classes, digits 0-9. We resized the resolution of these images to  $28 \times 28$  and converted the RGB images to gray-scale. 20% of this dataset is used as the test dataset (413 images) and the remaining images are used for validation, 330 images, and training. Figure 1 (c) shows a sample image for each class.

### 3. Model Design

We use three CNN models and a multi-layer perceptron (MLP) neural network for the static ASL image classification task. The CNN models are inspired by three standard and well-known models, i.e., LeNet, AlexNet, and VGGNet. Here, we slightly modified these models to create smaller versions that still achieve high accuracy values. Moreover, we constrained the models such that they could be readily converted to SNN models. The specifics for each implementation are provided in the following subsections.

#### 3.1. MLP

Figure 2a shows the structure of the MLP that we used in this work. The proposed MLP contains two hidden layers with 512 and 256 neurons each, as well as 24 and 10 output layers for ASL alphabet and ASL digits datasets, respectively. The first and second layers are followed by a dropout layer each with a probability of 0.2. We use the ReLU activation function for the hidden layers and the softmax activation function for the output layer.

#### 3.2. LeNet

The architecture of the LeNet [34] model that we employed here is shown in figure 2b. It is comprised of two convolutional layers and three fully connected layers. The first and second convolution layers consist of 6 and 16 kernels of size  $5 \times 5$ , respectively. After the first and second convolution layers, there is a non-overlapping average pooling layer with a  $2 \times 2$  filter size and strides of 2. The three fully-connected layers each include 120, 84, and 24 or 10 neurons depending if the ASL Alphabet or Digits are used. In this study, we modified the original LeNet model and applied two dropout layers with a probability of 0.25 to prevent overfitting after the first and the second fully-connected layers.

#### 3.3. AlexNet

The AlexNet model [35] consists of five convolutional layers each followed by max pooling and 3 fully connected (FC) layers, all of which utilize the ReLU activation function except the output layer, which employs the softmax activation function. The original AlexNet model is quite large, with over 62 million parameters. Here, we changed the structure of the original network as follows. Instead of 96  $11 \times 11$  kernels with a stride of

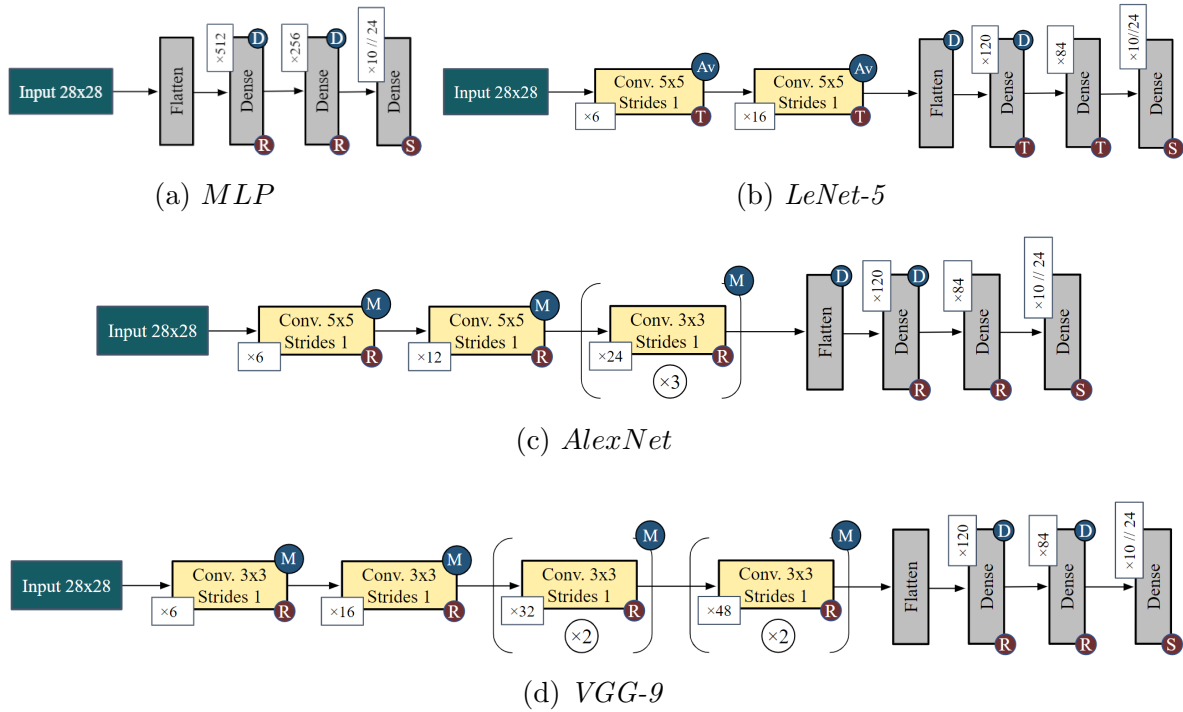


Figure 2: ANN Architectures for the ASL Alphabet (24 output classes) and ASL Digits (10 output classes) classification. **R** ReLU, **T** Tanh, **M** MaxPooling2D, **Av** AveragePooling2D, **D** Dropout, **S** Softmax.

4, just 6  $5 \times 5$  kernels with a stride of 1 are used for the first convolution layer. Instead of 256 kernels, we employ 12  $5 \times 5$  kernels for the second convolution layer. We utilize 24 kernels with a size of  $3 \times 3$  for each of the next three convolution layers. In the three FC layers, we employ 120, 84, and 24 or 10 neurons. To avoid overfitting, we apply dropout to fully-connected layers with a probability of 0.5 similar to the original AlexNet. Figure 2c shows the designed AlexNet-inspired architecture.

### 3.4. VGGNet

Another well-known CNN used herein is VGGNet [36], which employs several  $3 \times 3$  filters instead of larger filters like AlexNet [35]. VGGNet, like AlexNet, uses ReLU activation functions in the network’s hidden layers. Depending on the number of layers, there are multiple variations of VGG architecture. VGG-16, for example, includes 16 layers and about 138 million parameters. Figure 2d depicts the structure of the VGG-inspired model developed in this work. We utilize only 9 layers consisting 6 convolution layers, and 3 fully-connected layers. We choose 6 kernels for the first layer, 16 kernels for the second layer, 32 kernels for the third and fourth layers, and 48 kernels for the fifth and sixth layers. A non-overlapping max pooling layer with a  $2 \times 2$  filter size and strides of 2 follow each convolution block. For the dense layer, we use the same number of neurons

as AlexNet and LeNet models.

### *3.5. Model training*

The proposed models are trained using TensorFlow 2.6.2 [37] with a categorical crossentropy loss function, a batch size of 128 and the Adam optimizer with a learning rate of 0.001 on the ASL Alphabet and ASL Digits datasets for 50 and 400 epochs, respectively. The intensities of the input images are normalized from 0-255 to 0-1. Furthermore, data augmentation is utilized, which involves randomly rotating images in the range of 10 degrees, randomly shifting images horizontally and vertically by 10%, and randomly zooming images by 10%. During training, the best epoch is saved for each of the proposed models based on the lowest validation loss. Metrics like accuracy, precision, recall, and F1 score are used to evaluate the models.

## **4. SNN Conversion Toolbox Background**

The SNN Conversion Toolbox proposed in [25] was designed with flexibility in mind to enable ANN models to be automatically converted to SNNs [25]. During the SNN conversion process the toolbox performs several different steps:

- (i) Parse the trained ANN model along with the trained weights and activation values.
- (ii) Normalize, scale, and set the spiking neuron parameters such as the membrane potential thresholds, biases, and weights.
- (iii) Convert the layers of the ANN model into equivalent spiking representations using methods such as convolution unrolling.
- (iv) Deploy the resulting SNN on neuromorphic hardware or use a SNN simulator.

The SNN Conversion Toolbox employs rate-based encoding which generates input spike trains with regular spiking frequencies over a duration parameter set in toolbox configuration settings. According to the SNN Conversion Toolbox documentation [38] this duration value correlates to the number of timesteps that each input is exposed to the SNN during inference. Thus the length of an input spike train is equal to this duration. These spike trains then propagate through the network causing neurons in the SNN to fire if the neuron membrane potential is driven to or above its threshold. Then in the final layer, the classification layer, the neuron which fires the most is taken as the output class. These steps are a high level view of the SNN Conversion Toolbox's ANN conversion methodology. Refer to [25] for detailed information on the methodologies used during the conversion process.

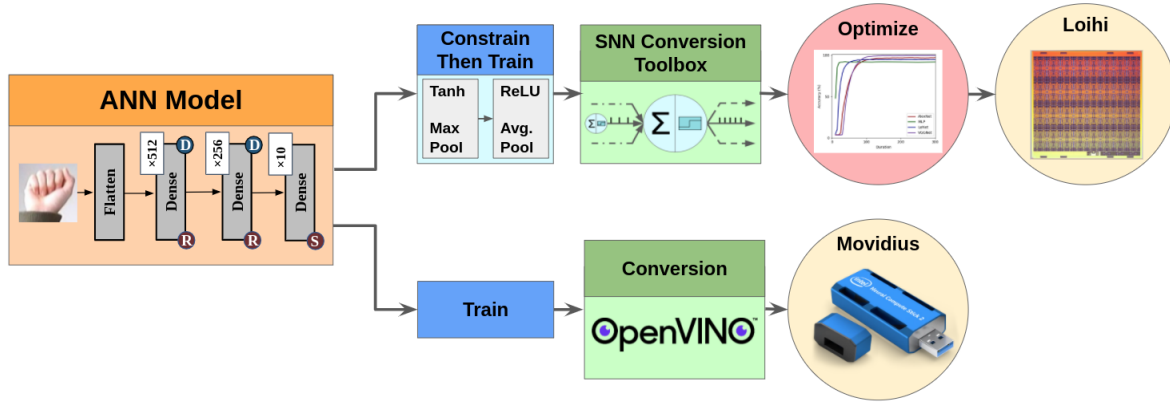


Figure 3: Experimental methodology for ASL classification on Intel NCS2 and Loihi.

## 5. Experiment Methodology

Now that neuromorphic hardware, such as Intel’s Loihi [24], is becoming more readily available to researchers, SNNs can now be designed and tested on hardware specifically designed to accelerate SNNs. This allows SNNs to be fairly compared against their DNN counterparts on conventional hardware accelerators like GPUs and TPUs [39,40].

In this work, we deploy our developed ANN and SNN models on the Intel Neural Compute Stick 2 (NCS2) and the Intel Loihi neuromorphic hardware, respectively. Our experimental methodology is depicted in Figure 3. In particular, the Loihi experiments were performed on four Loihi chips for accuracy measurements and a board of 32 Loihi chips called Nahuku-32 for power measurements. Each of the models in Figure 2 were deployed on Loihi and NCS2 using the SNN Conversion Toolbox and OpenVINO APIs, respectively. From there, the performance of each hardware platform was measured with respect to latency, power, and accuracy.

### 5.1. Intel Neural Compute Stick 2

The Intel Neural Compute Stick 2 (NCS2) is based on the Intel Movidius X Vision Processing Unit (VPU), which has 16 programmable SHAVE cores and a dedicated neural compute engine for hardware acceleration of deep neural network inferences. It features a base frequency of 700 MHz with a 16 nm technology node. Additionally, NCS2 has 4 GB memory with maximum frequency of 1600 MHz. NCS2 supports 16-bit floating point operations, which we have found to be sufficient for our ASL classification tasks [41].

**5.1.1. Conversion:** To deploy the ANN models on NCS2, Intel provides a Python3 and C library called OpenVINO. Specifically, we used OpenVINO 2022.1.4 for our experiments. To deploy the models to the NCS2, the TensorFlow trained models were first frozen using TensorFlow’s `get_concrete_function()` and `convert_variables_to_constants_v2()` functions. From these frozen models, the



Table 1: Loihi Platforms.

Node	Chips	x86 Cores	Neurocores	Neurons	In-Axons	Out-Axons	State Memory
Loihi	4	12	512	524,288	2,097,152	2,097,152	65,536 KB
Nahuku-32	32	96	4096	4,194,304	16,777,216	16,777,216	524,288 KB

OpenVINO model optimizer was used to convert the models to a format which enables their deployment to run on the NCS2. Once the model is optimized for Intel NCS2, we then used the inference engine API built into OpenVINO to perform inference and subsequently measure the accuracy, latency, and power.

*5.1.2. Latency and Power Measurement:* Using OpenVINO, we performed 10 iterations over the entire test datasets, 7172 images for the ASL Alphabet dataset and 413 images for the ASL Digit dataset. The latencies were recorded over the 10 iterations for each image and then averaged at the end. We used a USB 3.0 measurement tool (MakerHawk UM34C [42]) along with a phone application to measure and record the power of the NCS2. This measurement device captures the overall system power usage, including USB I/O, due to its inline nature. The power measurement tool was attached to a computer’s USB port along with the NCS2 and the idle and running power were recorded. Idle power is recorded for 5 minutes after plugging the NCS2 into the UM34C and the computer, and the voltage and current are measured every second. We then perform inference on the entire testing dataset for 10 iterations and record the average running power. The difference between average running power and idle power is calculated as the *inference power*.

## 5.2. Intel Loihi

Each experiment was performed on Intel’s Neuromorphic Research Community’s (INRC) cloud infrastructure setup for INRC members to test models on Intel’s Loihi platform. In particular, two different nodes in the INRC cloud were used, one consisting of four Loihi chips and the other, Nahuku-32, consisting of 32 Loihi chips combined on a single board [23]. Each Loihi neuromorphic core or neuro-core can simulate up to 1024 spiking neurons or compartments, 4096 fan-out axons, 4096 fan-in axons, and 128 kilobytes of fan-in state memory [24]. The details of each Loihi platform node in the INRC cloud infrastructure are provided in Table 1.

*5.2.1. Conversion Methodology:* In 2021, NxTF [30] was released which enabled the SNN Conversion Toolbox [25] to convert a trained ANN model to an SNN and allow it to be deployed on Intel’s Loihi platform. The SNN Conversion toolbox, while supporting many of the common layers found in CNNs, does not support some ANN components and layers on Loihi. To combat this, we employ a constraint-then-train method to ensure compatibility with the Loihi backend for the SNN Conversion Toolbox before conversion.

Table 2: ASL Alphabet Model Parameters and Loihi Core Partitioning

Layer	MLP		LeNet		AlexNet		VGGNet	
	Param	Loihi Cores	Param	Loihi Cores	Param	Loihi Cores	Param	Loihi Cores
Conv1	-	-	156	9	156	12	60	12
Conv2	-	-	2416	4	1812	7	880	7
Conv3	-	-	-	-	2616	3	4640	4
Conv4	-	-	-	-	5208	4	9248	7
Conv5	-	-	-	-	5208	4	13872	2
Conv6	-	-	-	-	-	-	20784	3
FC1	401920	10	30849	1	26040	1	5880	1
FC2	131328	4	10164	1	10164	1	10164	1
Output	6168	1	2040	1	2040	1	2040	1
<b>Total</b>	<b>539,416</b>	<b>18</b>	<b>45,616</b>	<b>21</b>	<b>53,244</b>	<b>41</b>	<b>67,568</b>	<b>47</b>

Table 3: ASL Digits Model Parameters and Loihi Core Partitioning

Layer	MLP		LeNet		AlexNet		VGGNet	
	Param	Loihi Cores	Param	Loihi Cores	Param	Loihi Cores	Param	Loihi Cores
Output	2570	1	850	1	850	1	850	1
<b>Total</b>	<b>535,818</b>	<b>18</b>	<b>44,426</b>	<b>21</b>	<b>52,054</b>	<b>41</b>	<b>66,378</b>	<b>47</b>

The constrain-then-train method consists of first replacing all max-pooling layers with average-pooling layers and then changing the activation functions from *TanH* to *ReLU*. We then train the models with the same configuration as before and then input the trained models into the SNN Conversion Toolbox.

As mentioned in Section 4, after the trained ANN is converted to an SNN, the SNN Conversion Toolbox uses the parameters and layer information from the SNN to deploy the models on neuromorphic hardware or a software simulator. In this case, the toolbox uses the information about the converted SNN layers and structure to appropriately partition the Loihi neuro-cores. This partitioning process is described in [30] and consists of optimization techniques which ensure that the neuro-cores can efficiently communicate. The specific number of neuro-cores which were partitioned for each layer of our converted SNN models can be seen in Tables 2 and 3. Once the partitioning process has succeeded, the SNN Conversion Toolbox proceeds to deploy the SNN on Loihi and begins performing inferences on the test dataset.

*5.2.2. Latency and Power Measurement:* After designing the ANNs using the aforementioned constrain-then-train method and converting them to SNNs, we performed multiple experiments with varying durations, a hyper-parameter defined in Section 4. Duration values were then chosen to achieve one of two different objectives: to attain high accuracy without duration considerations or to achieve a balance between duration and accuracy. To collect the latency and power measurements, we set the *profile\_performance* output configuration setting in the toolbox while targeting the Nahuku-32 board. Nahuku-32 was chosen since it contains the necessary power and latency recording hardware [23]. While the Nahuku-32 board contains 32 Loihi chips, Tables 2 and 3 show that the SNN models tested do not allocate more than the 128 neuro-cores in a single chip. Therefore, it can be inferred that only a single Loihi chip was allocated for all of the models. For each of the varying durations, the latency and power metrics were recorded when the SNN models were deployed on the Nahuku-32 board. After completing all inferences, the toolbox then reports the power usage for the neuro-cores, x86 cores, and the total system power. For each model, power measurements for various duration values were averaged together to attain a typical power usage of the model on Loihi regardless of the duration.

## **6. Results**

In this section, we compare the SNNs' and ANNs' performance in terms of accuracy, latency, power, and energy consumption. We also provide insights into the techniques utilized to obtain high SNN accuracy and then provide an analysis on the balance between accuracy and latency. Finally, the SNN on Loihi is compared to the ANN on Intel NCS2 in terms of latency, power, and energy.

### *6.1. Accuracy Analysis*

SNNs have been shown in previous works to have comparable if not better accuracy than ANNs due to the introduction of noise by the nature of spikes approximating the floating point values in an ANN [40, 43]. Tables 4 and 5 show the overall accuracy and macro-averaged F1-score values obtained for the ANN, constrained ANN (C-ANN), and SNN models for the ASL Alphabet and ASL Digits, respectively.

Table 4: Accuracy of ANN, Constrained-ANN (C-ANN), and SNN models for ASL Alphabet dataset.

Architecture	Accuracy			Macro-Average		
	(%)			F1-Score (%)		
	ANN	C-ANN	SNN	ANN	C-ANN	SNN
MLP	92.24	-	92.07	91.65	-	91.28
LeNet	98.93	96.44	94.87	98.96	96.10	94.22
AlexNet	98.68	98.91	96.88	98.48	98.50	96.08
VGGNet	99.60	99.46	99.44	99.56	99.45	99.40

Table 5: Accuracy of ANN, Constrained-ANN (C-ANN), and SNN models for ASL Digits dataset.

Architecture	Accuracy			Macro-Average		
	(%)			F1-Score (%)		
	ANN	C-ANN	SNN	ANN	C-ANN	SNN
MLP	86.19	-	86.92	86.30	-	86.89
LeNet	98.55	97.09	97.34	98.48	97.04	97.27
AlexNet	99.03	98.06	98.79	99.05	97.08	98.84
VGGNet	99.03	99.27	99.52	99.09	99.28	99.51

First we compare the ANN versus C-ANN model accuracies and F1-scores before conversion. As listed in Tables 4 and 5, the VGGNet ANN and C-ANN models achieve the highest values for accuracy and F1-score. In particular, for the ASL Alphabet, the VGG ANN realizes the best accuracy of 99.60% and F1-score of 99.56%, while for ASL digits, the VGG C-ANN has the best accuracy and F1-score at 99.27% and 99.28%. For both datasets, the ASL Alphabet and Digits, the MLP networks performed the worst with the lowest accuracies and F1-scores. Since the MLP models did not contain any *TanH* activations or pooling layers, no constrained models were created, and thus, the C-ANN metrics have been left empty. We can also see that the AlexNet C-ANN on the ASL Alphabet performs marginally better when compared to the conventional ANN with a 0.23% and 0.02% difference in accuracy and F1-score, respectively.

In Tables 4 and 5, we also present the accuracies and F1-scores obtained from the deployed SNN models run on the durations which maximize accuracy. In Table 4, the VGGNet SNN achieves the best SNN accuracy of 99.44% and F1-score of 99.40% compared to the other SNN architectures. This also holds true for the ASL Digits

dataset in Table 5 where the highest SNN accuracy and F1-score is 99.52% and 99.51%, respectively. Comparing the ANN and SNN models, the ASL Alphabet VGGNet SNN loses just 0.16% of its accuracy after conversion. However for the ASL Digits, the VGG SNN actually outperforms both the ANN and C-ANN in terms of accuracy and F1-score gaining an additional 0.25% accuracy over the C-ANN and 0.49% over the ANN. A similar pattern can be seen for the ASL Digits’ LeNet and MLP SNNs where the LeNet SNN gains 0.25% over the C-ANN and the MLP SNN gains 0.73% over the ANN. However, in the LeNet ASL Digit SNN the accuracy is still lower than the ANN. The differences between the alphabet C-ANN and SNN for MLP, LeNet, and AlexNet are 0.17%, 1.57%, and 2.03%, respectively, marginally favoring the C-ANN. Similar to the ANNs, the MLP SNNs for both datasets have the lowest accuracies and F1-scores. The stated accuracies for the SNN models in Tables 4 and 5 are acquired for longer duration values to maximize accuracy. These durations are shown later in Table 7 and 8 for the ASL Alphabet and Digits datasets, respectively.

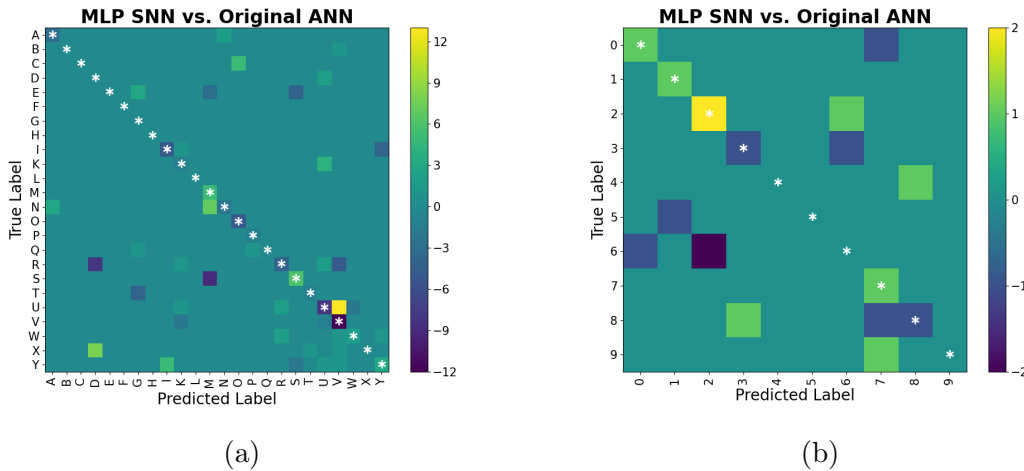


Figure 4: MLP Difference Confusion Matrices for (a) ASL Alphabet and (b) ASL Digits. See Figures B1 and B2 in Appendix B for the other models.

To provide more detailed information about the accuracy of the models, Figure 4 (and Appendix B) exhibit difference confusion matrices for the original ANN versus the SNN and the C-ANN versus the SNN. These figures are dubbed “difference” confusion matrices because they represent the difference between two models. When the color value of a pixel is close to zero on the color scale, this conveys that the SNN and ANN or C-ANN were about equal in their performance. The diagonals of these difference matrices are emphasized with white asterisks to show where the SNN and ANN correctly classified the input. If a pixel on the diagonal is bright yellow then the SNN correctly classified more inputs than the ANN or C-ANN. However, if the pixel on the diagonal is dark blue or purple the ANN or C-ANN was more accurate than the SNN at classifying the input. If the pixel does not lie on the diagonal of the matrix and is yellow then this concludes that the SNN was more incorrect than the ANN or C-ANN and vice-versa.

### 6.2. Latency

As mentioned in Section 4, the duration parameter is the number of timesteps that each input is exposed to the SNN. Thus, modifying this duration value should have a linear affect on the inference latency. As mentioned in Section 5.2.2, the Nahuku-32 board does contain the power and latency measurement hardware, but the polling is limited to a 30-40ms time resolution [44]. This limit, thus, prevents the power and latency measurements when running on lower values of duration. To mitigate the polling issue, we performed our experiments using a set of higher and uniformly distributed values of duration to drive the time for inference above the 30-40ms threshold. For each of the higher durations, the models are run and the latency is recorded and plotted seen as red circles ● on the graphs in Figure 5 (and the figures in Appendix A). From there, the least squares method was used to generate the line of best fit. As seen in the graphs of Figure 5 (and in Appendix A), the relationship between duration and latency is roughly linear for all the models on higher durations. Thus, from here on, we use the fitted line to obtain the SNN inference latency for various duration values.

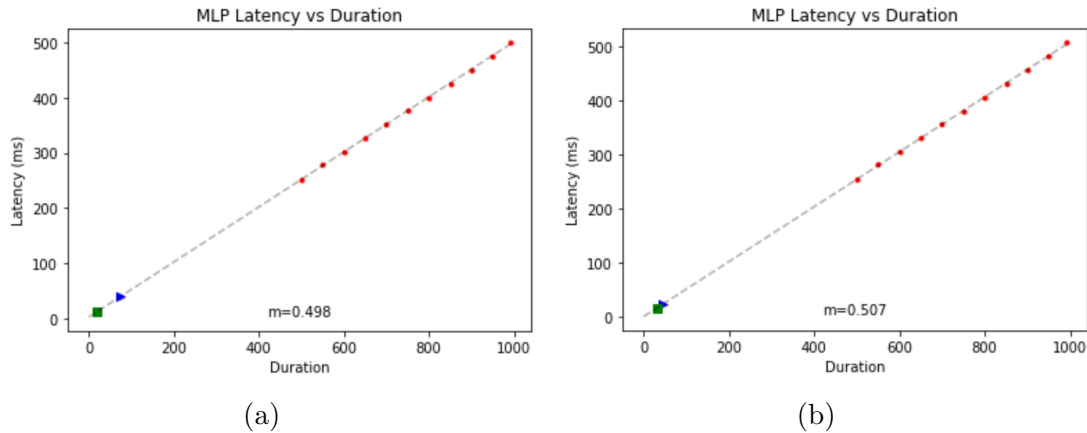


Figure 5: MLP Latency vs. Duration graphs for (a) ASL Alphabet and (b) ASL Digit dataset. See Appendix Appendix A for the other models. Legend: ● test points, ▲ best accuracy, ■ balanced duration-accuracy point.

*6.2.1. Loihi Accuracy and Duration/Latency Balance:* As shown in Figure 6, for various SNN models run on Loihi, as the duration/latency increases so does accuracy. However, after a specific duration, the accuracy plateaus and there is little to no gain in accuracy at the cost of significantly increasing duration and therefore latency. Thus, we aim to find a balance between the accuracy and duration such that we can achieve and acceptable accuracy while reducing the latency.

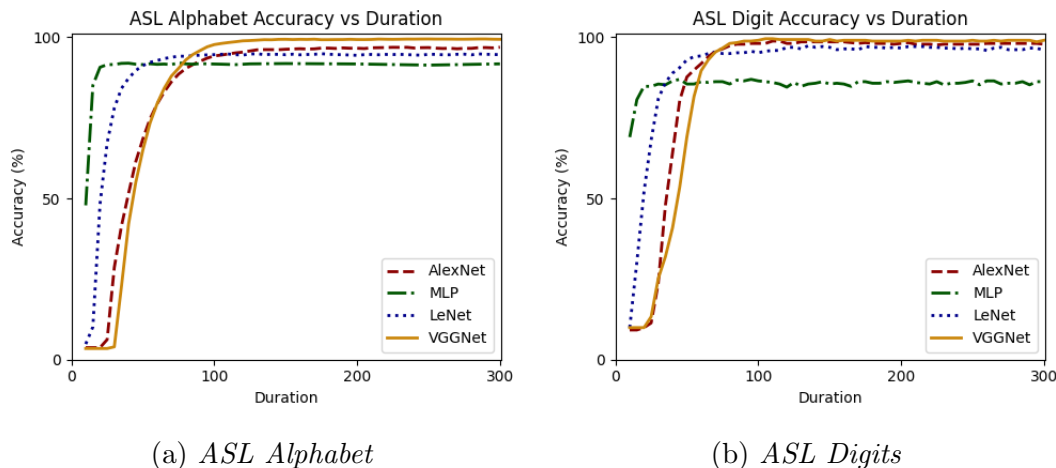


Figure 6: Accuracy-Duration Tradeoff. The SNN model’s accuracy on test dataset is related to the number of timesteps in which each sample is given.

The blue triangles  $\blacktriangle$  on the graphs in Figure 5 (and the figures in Appendix A) represent the maximum possible accuracy for the respective models between 0 and 300 duration timesteps with increments of 5. The quantitative values of the blue point can be found as the “Best Accuracy” metrics in Table 6 as well as the SNN accuracy values in Tables 4 and 5 previously mentioned in Section 6.1. While it is possible that a higher accuracy could be achieved after 300 duration timesteps, this accuracy would incur a significantly higher inference latency.

Table 6 demonstrates the accuracy and duration trade-offs, for multiple relaxed accuracy values ranging from 1.0% to 5.0% accuracy reductions. As seen in Table 6 there are significant reductions in duration if a small reduction in accuracy is allowed.

Table 6: Relaxed accuracy yielding lower duration.

Dataset	SNN Model	Best Accuracy	Accuracy Drop Ranges					
			0.0%	<1.0%	<2.0%	<3.0%	<4.0%	<5.0%
Alphabet	MLP	92.07%	75	25	20	20	20	20
	LeNet	94.87%	130	75	65	55	50	50
	AlexNet	96.88%	300	130	115	100	95	90
	VGGNet	99.44%	250	115	100	95	90	85
Digits	MLP	86.92%	45	40	30	20	20	20
	LeNet	97.34%	135	120	70	65	55	50
	AlexNet	98.79%	110	85	80	75	70	65
	VGGNet	99.52%	105	90	80	75	75	70

In Table 7 and 8, we chose the duration point from Table 6 where the accuracy drop is no more than 2.0%. This threshold was chosen because it reduces the duration, therefore the latency, without significantly reducing the accuracy. However, another

accuracy threshold can be chosen depending on the application’s sensitivity to accuracy or latency. The green squares ■ on the graphs in Figure 5 (and the graphs in Appendix A) exhibit the 2.0% relaxed accuracy point. The accuracy, duration, and latency values for this point are provided in Tables 7 and 8 as the “Balanced Point” metrics.

Table 7: ASL Alphabet SNN best accuracy metrics versus metrics for balanced accuracy-duration on Loihi.

SNN Model	Best Point ▲			Balanced Point ■		
	Duration	Latency (ms)	Accuracy (%)	Duration	Latency (ms)	Accuracy (%)
MLP	75	40.06	92.07	20	12.64	90.67
LeNet	130	13.21	94.87	65	8.97	93.39
AlexNet	300	20.69	96.88	115	11.40	95.13
VGGNet	250	14.03	99.44	100	8.03	97.70

Table 8: ASL Digit SNN best accuracy metrics versus metrics for balanced accuracy-duration on Loihi.

SNN Model	Best Point ▲			Balanced Point ■		
	Duration	Latency (ms)	Accuracy (%)	Duration	Latency (ms)	Accuracy (%)
MLP	45	23.89	86.92	30	16.29	85.47
LeNet	135	13.56	97.34	70	9.67	95.40
AlexNet	110	10.67	98.79	80	9.04	97.34
VGGNet	105	8.72	99.52	80	7.77	98.06

As listed in Tables 7 and 8, the balanced point’s latency is significantly reduced compared to that of the best accuracy point. The ASL Alphabet appears to benefit the most from the accuracy-duration balancing. As seen in Table 7, the MLP’s SNN accuracy drops just 1.4% but the duration decreases by 73.33% equating to a 68.44% drop in latency. VGGNet’s accuracy is reduced by 1.74% after balancing, from 99.44% to 97.70%, and the duration is subsequently reduced by 60.0% and latency by 42.77%. The accuracy loss for the other two models, LeNet and AlexNet, is 1.48% and 1.75%, respectively. Their duration reduction is 50.0% and 61.67% equating to a latency reduction of 32.10% and 44.90%, respectively.

For the ASL Digits dataset, the MLP SNN has the most significant difference in duration and latency with a 31.81% reduction in latency and a 1.45% drop in accuracy. The duration reductions for LeNet, AlexNet, and VGGNet are 48.15%, 27.27%, and 23.81%, while the accuracy loss is 1.94%, 1.45%, and 1.46%, respectively. The latency reduction for the three SNN models are thus 28.69%, 15.28%, and 10.89%, respectively. Hence, for applications that can tolerate more error, it is self-evident that lower latency configurations can be employed.



Table 9: Movidius vs Loihi power comparison on ASL Alphabet

Model	Movidius Power (mW)		Loihi Power (mW)					
	Idle	Running	X86 Cores			Neuro-cores		
			Static	Dynamic	Total	Static	Dynamic	Total
MLP	635	1513	0.254	18.180	18.434	15.440	27.500	42.940
Lenet	635	1487	0.255	18.736	18.991	18.119	20.954	39.073
AlexNet	635	1482	0.263	18.806	19.069	36.423	23.595	60.018
VGGNet	635	1460	0.253	19.037	19.290	40.180	12.422	52.602

Table 10: Movidius vs Loihi power comparison on ASL Digits

Model	Movidius Power (mW)		Loihi Power (mW)					
	Idle	Running	X86 Cores			Neuro-cores		
			Static	Dynamic	Total	Static	Dynamic	Total
MLP	635	1484	0.255	18.187	18.442	15.476	26.312	41.788
Lenet	635	1473	0.262	18.835	19.097	18.602	22.831	41.433
AlexNet	635	1472	0.258	18.848	19.106	35.699	35.535	71.234
VGGNet	635	1475	0.267	18.964	19.231	42.423	22.890	65.313

### 6.3. Intel Loihi and NCS2 Compared

Here, we compare the performance of ANNs on Intel’s NCS2 with the performance of SNNs on Intel’s Loihi neuromorphic chips in terms of latency, power, and energy.

To measure the inference power consumption on Loihi, the accuracy-latency balanced SNN models discussed in the previous subsection are evaluated on the Nahuku-32 board. The LeNet SNN, for the ASL Alphabet, and MLP SNN, for the ASL Digits, have the lowest inference power with 58.064 mW and 60.230 mW, respectively. The AlexNet SNN, on the other hand, has the highest inference power, with the ASL Alphabet and ASL Digits inference powers of 79.087 mW and 90.340 mW, respectively (see Tables 9 and 10). For NCS2, an idle power of 635 mW is measured using the method discussed in Section 5.1.2. The MLP network has somewhat higher inference power for both datasets compared to all other models running on NCS2, with 878 mW and 849 mW for the ASL Alphabet and ASL Digits, respectively. On the other hand, VGGNet has the lowest inference power on ASL Alphabet, with an inference power of 825 mW. On ASL Digits, however, the CNN architectures have very comparable inference power. In terms of latency, the MLP on the NCS2 has the least latency for both ASL Alphabet and ASL digits, with 2.125 ms and 2.057 ms values, respectively, whereas VGGNet has the greatest latency, with values of 2.593 ms and 2.470 ms, respectively. On both datasets, on Loihi, the VGGNet SNN had the least inference latency. The SNN models running on Loihi, in general, have a greater inference latency, ranging from 8.03 ms to 12.64 ms for the ASL alphabet and 7.77 ms to 16.29 ms for the ASL digits. This higher latency, when compared to NCS2, can be attributed to the inclusion of three x86 cores in

the current implementation of Loihi [23]. The x86 cores introduce a substantial amount of latency into the system due the current sub-optimal implementation of the cores in the Loihi system and the communication differences between a synchronous computation on the x86 cores and asynchronous computation on the neuro-cores [23]. This latency issue should be improved upon in the upcoming newest iteration of the Loihi neuromorphic hardware, Loihi 2.

In terms of inference energy consumption, the LeNet SNN model on Loihi has the lowest inference energy, with 0.521 mJ and 0.585 mJ for the ASL Alphabet and ASL Digits, respectively. On the ASL Alphabet images, the VGGNet SNN model on Loihi consumes only 0.056 mJ more energy than LeNet but achieves 4.31 % higher accuracy. VGGNet also consumes 0.072 mJ more inference energy for the ASL Digits, although it is 2.66% more accurate compared to the LeNet SNN. As a result, the VGGNet SNN is the more appropriate choice for applications that require a model with high accuracy and low energy consumption.

A comprehensive comparison of the SNN models implemented on Loihi and ANN models deployed on NCS2 is provided in Tables 11 and 12. All of the SNN models on Loihi use less power and energy compared to ANN models. On the ASL Alphabet, for example, while VGGNet loses just 1.9% accuracy after converting from the ANN to a SNN, it consumes  $11.48\times$  less inference power and  $3.71\times$  less inference energy. For the ASL Digits dataset, the VGGNet SNN running on Loihi consumes  $9.94\times$  less inference power and  $3.16\times$  lower energy compared to VGGNet ANN on NCS2.

Table 11: Movidius vs Loihi - Comprehensive Analysis - ASL Alphabet

Benchmarking Metric	Movidius				Loihi			
	MLP	LeNet	AlexNet	VGGNet	MLP	LeNet	AlexNet	VGGNet
Accuracy (%)	92.24	98.93	98.68	99.60	90.67	93.39	95.13	97.70
Inference Power (mW)	878	852	857	825	61.373	58.064	79.087	71.892
Latency (mS)	2.125	2.503	2.588	2.593	12.64	8.97	11.40	8.03
Inference Energy (mJ)	1.866	2.133	2.218	2.139	0.776	0.521	0.902	0.577

Table 12: Movidius vs Loihi - Comprehensive Analysis - ASL Digits

Benchmarking Metric	Movidius				Loihi			
	MLP	LeNet	AlexNet	VGGNet	MLP	LeNet	AlexNet	VGGNet
Accuracy (%)	86.19	98.55	99.03	99.03	85.47	95.40	97.34	98.06
Inference Power (mW)	849	838	837	840	60.230	60.530	90.340	84.544
Latency (mS)	2.057	2.287	2.391	2.470	16.29	9.67	9.04	7.77
Inference Energy (mJ)	1.746	1.916	2.001	2.075	0.981	0.585	0.817	0.657

## **7. Conclusion**

In this study, we first trained four different ANN models on two static ASL hand gesture image datasets, the ASL Alphabet and ASL Digits. We then modified and trained constrained versions of these models to ensure compatibility with the SNN Conversion Toolbox. We then deployed the converted SNNs on Intel’s neuromorphic processor, Loihi, and benchmarked them against their conventional ANN implementations on edge devices such as Intel NCS2 used herein. We then performed an analysis of the correlation between the accuracy and duration/latency of the SNN models and provided a method to find a balanced point according to an application’s requirements. Moreover, we discussed specific mechanisms to accurately measure the power consumption and latency in both neuromorphic and edge computing hardware. Finally, we provided a comprehensive comparison between Loihi and NCS2 in terms of accuracy, latency, power consumption, and energy. In terms of accuracy, the SNN models approach or even surpass ANN models. In terms of latency, Loihi falls behind Intel’s NCS2, however, the power reduction realized by Loihi is so significant (9.26-14.67 $\times$ ) that it could still achieve 1.78-4.09 $\times$  energy savings compared to NCS2 while executing the ASL classification tasks. Future work includes dynamic hand gesture recognition of ASL using temporal learning rules for SNNs.

## Appendix A. Duration vs. Latency

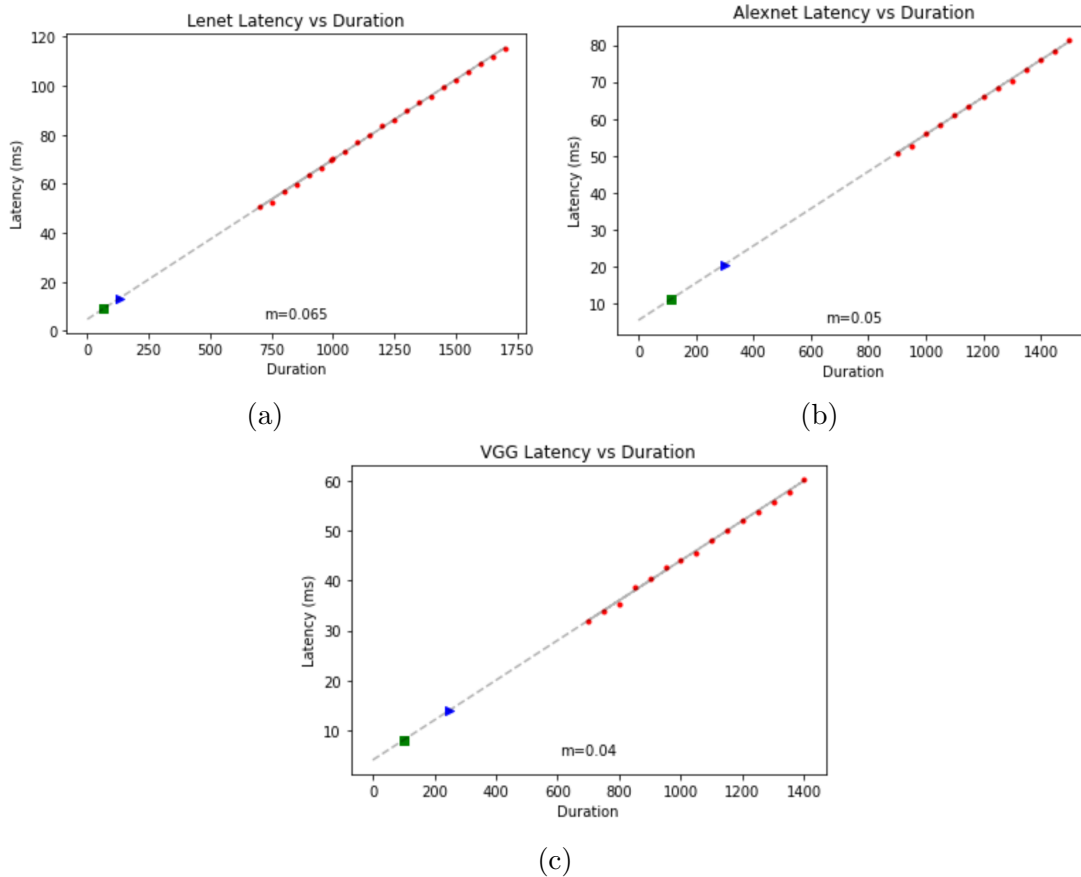


Figure A1: ASL Alphabet Latency vs. Duration. Legend: ● test points, ▲ best accuracy, ■ balanced duration-accuracy point.

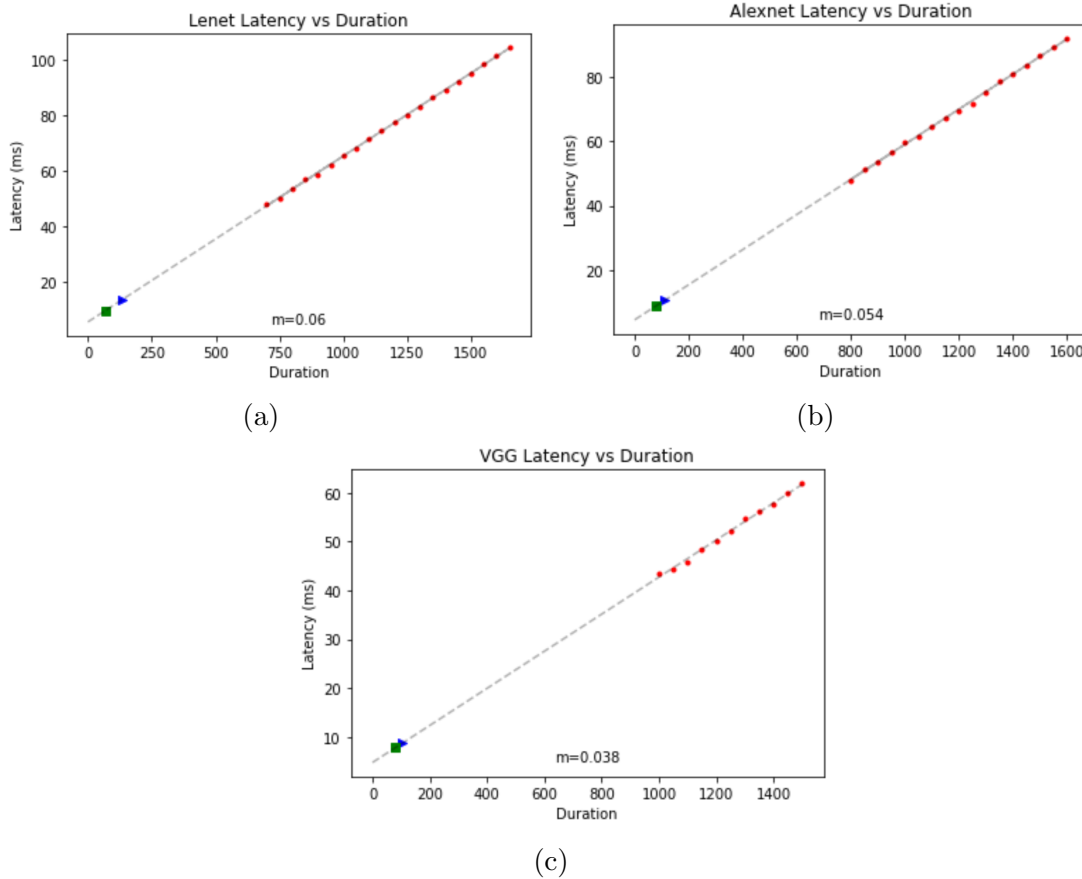


Figure A2: ASL Digits Latency vs. Duration. Legend: ● test points, ▲ best accuracy, ■ balanced duration-accuracy point.

Appendix B. Confusion Matrices

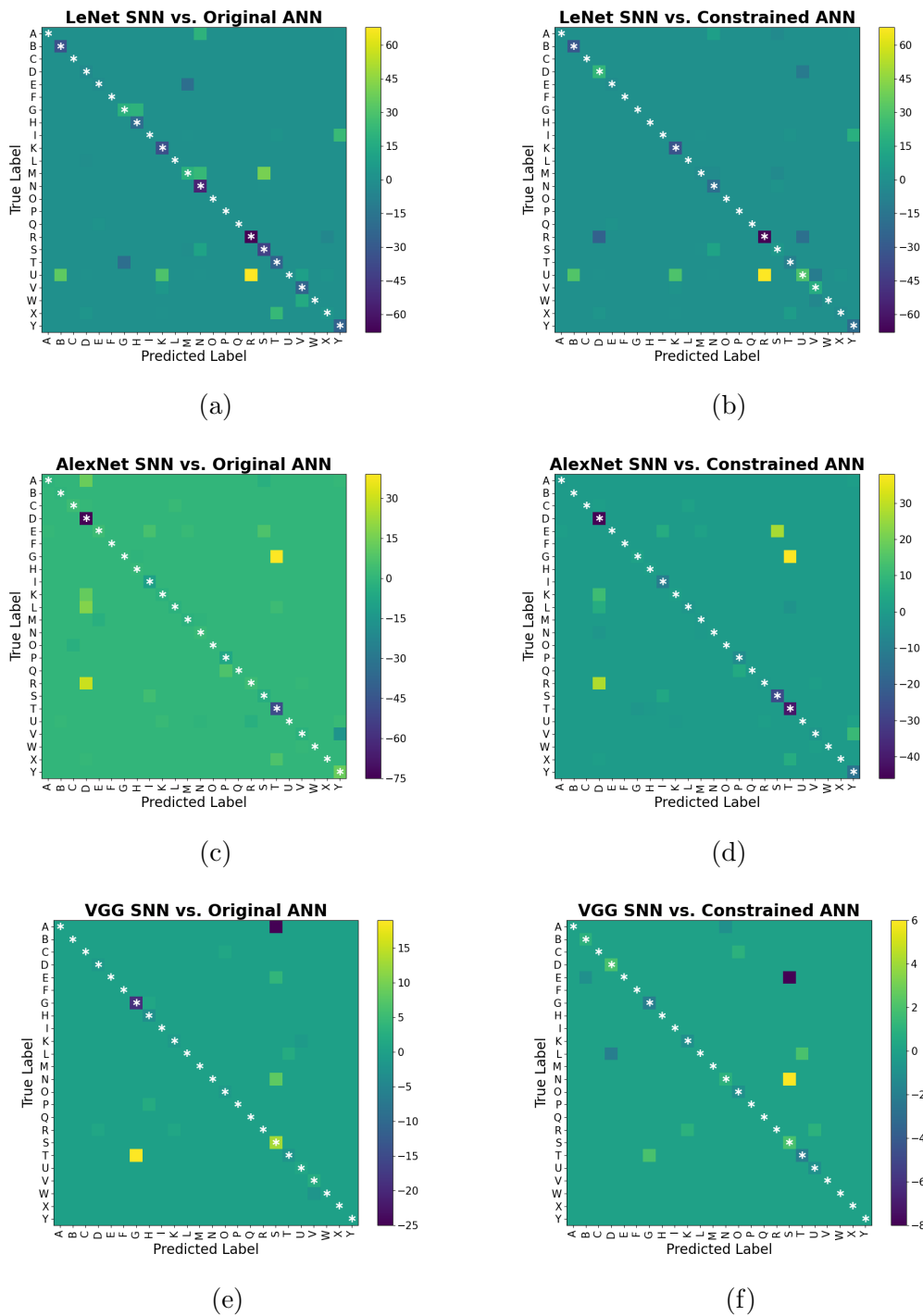


Figure B1: ASL Alphabet Difference Confusion Matrices.

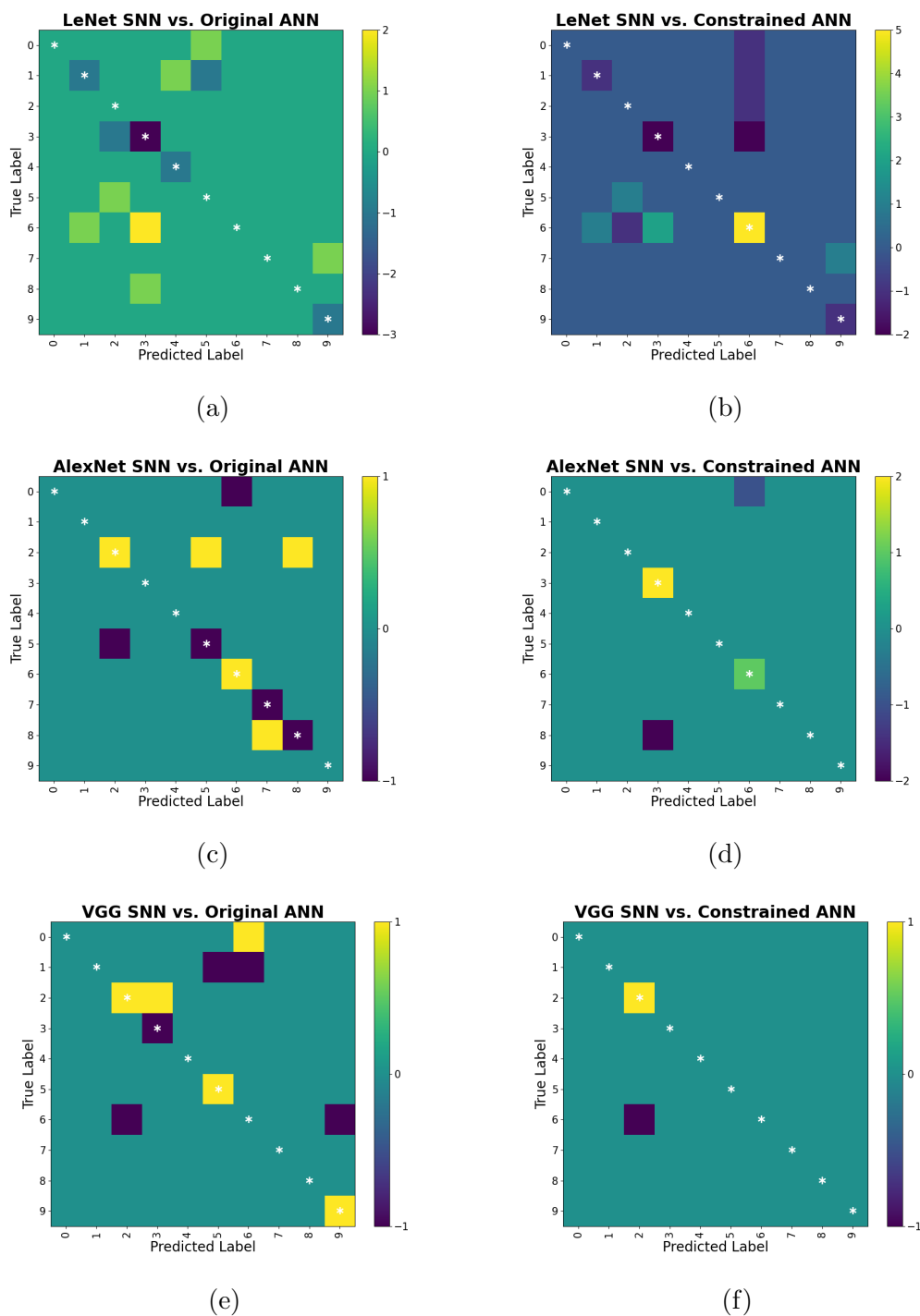


Figure B2: ASL Digits Difference Confusion Matrices.

### Acknowledgment

This work is partially supported by an ASPIRE grant from the Office of the Vice President for Research at the University of South Carolina. Special thanks to the Intel Neuromorphic Research Community (INRC) for providing access to the Loihi chips for

the experiments performed in this paper.

## References

- [1] Cheok M J, Omar Z and Jaward M H 2019 *International Journal of Machine Learning and Cybernetics* **10** 131–153
- [2] Tolentino L K S, Juan R O S, Thio-ac A C, Pamahoy M A B, Forteza J R R and Garcia X J O 2019 *International Journal of Machine Learning and Computing* **9** 821–827
- [3] Liao Y, Xiong P, Min W, Min W and Lu J 2019 *IEEE Access* **7** 38044–38054
- [4] Wadhawan A and Kumar P 2021 *Archives of Computational Methods in Engineering* **28** 785–813
- [5] Shukor A Z, Miskon M F, Jamaluddin M H, bin Ali F, Asyraf M F, bin Bahar M B *et al.* 2015 *Procedia Computer Science* **76** 60–67
- [6] Kumar P, Saini R, Behera S K, Dogra D P and Roy P P 2017 *2017 Fifteenth IAPR international conference on machine vision applications (MVA) (IEEE)* pp 157–160
- [7] Zhang X, Chen X, Li Y, Lantz V, Wang K and Yang J 2011 *IEEE Transactions on Systems, Man, and Cybernetics-Part A: Systems and Humans* **41** 1064–1076
- [8] Hernandez-Rebollar J L, Kyriakopoulos N and Lindeman R W 2004 *Sixth IEEE International Conference on Automatic Face and Gesture Recognition, 2004. Proceedings.* (IEEE) pp 547–552
- [9] Bui T D and Nguyen L T 2007 *IEEE sensors journal* **7** 707–712
- [10] ElBadawy M, Elons A S, Sheded H and Tolba M F 2015 *Intelligent Systems' 2014* (Springer) pp 721–730
- [11] Marin G, Dominio F and Zanuttigh P 2014 *2014 IEEE International Conference on Image Processing (ICIP)* pp 1565–1569
- [12] Kumar P, Gauba H, Roy P P and Dogra D P 2017 *Pattern Recognition Letters* **86** 1–8
- [13] Garcia B and Viesca S A 2016 *Convolutional Neural Networks for Visual Recognition* **2** 225–232
- [14] Rautaray S S and Agrawal A 2015 *Artificial intelligence review* **43** 1–54
- [15] Pisharady P K and Saerbeck M 2015 *Computer Vision and Image Understanding* **141** 152–165
- [16] D’Orazio T, Marani R, Renò V and Cicirelli G 2016 *Image and Vision Computing* **52** 56–72
- [17] Rastgoo R, Kiani K and Escalera S 2018 *Entropy* **20** 809
- [18] Adithya V and Rajesh R 2020 *Procedia Computer Science* **171** 2353–2361
- [19] Barbhuiya A A, Karsh R K and Jain R 2021 *Multimedia Tools and Applications* **80** 3051–3069
- [20] Rahman M M, Islam M S, Rahman M H, Sassi R, Rivolta M W and Aktaruzzaman M 2019 *2019 International Conference on Sustainable Technologies for Industry 4.0 (STI) (IEEE)* pp 1–6
- [21] Verhelst M and Moons B 2017 *IEEE Solid-State Circuits Magazine* **9** 55–65
- [22] Schuman C D, Kulkarni S R, Parsa M, Mitchell J P, Kay B *et al.* 2022 *Nature Computational Science* **2** 10–19
- [23] Davies M, Wild A, Orchard G, Sandamirskaya Y, Guerra G A F, Joshi P, Plank P and Risbud S R 2021 *Proceedings of the IEEE* **109** 911–934
- [24] Davies M, Srinivasa N, Lin T H, Chinya G, Cao Y, Choday S H, Dimou G, Joshi P, Imam N, Jain S, Liao Y, Lin C K, Lines A, Liu R, Mathaikutty D, McCoy S, Paul A, Tse J, Venkataramanan G, Weng Y H, Wild A, Yang Y and Wang H 2018 *IEEE Micro* **38** 82–99
- [25] Rueckauer B, Lungu I A, Hu Y, Pfeiffer M and Liu S C 2017 *Frontiers in Neuroscience* **11** ISSN 1662-453X URL <https://www.frontiersin.org/article/10.3389/fnins.2017.00682>
- [26] Pérez-Carrasco J A, Zhao B, Serrano C, Acha B, Serrano-Gotarredona T, Chen S and Linares-Barranco B 2013 *IEEE Transactions on Pattern Analysis and Machine Intelligence* **35** 2706–2719
- [27] Cao Y, Chen Y and Khosla D 2015 *International Journal of Computer Vision* **113** 54–66 URL <https://doi.org/10.1007/s11263-014-0788-3>
- [28] Abadi M, Barham P, Chen J, Chen Z, Davis A *et al.* 2016 *12th USENIX Symposium on Operating Systems Design and Implementation (OSDI 16)* (Savannah, GA: USENIX Association) pp 265–283 ISBN 978-1-931971-33-1



- [29] Paszke A, Gross S, Massa F, Lerer A, Bradbury J, Chanan G, Killeen T, Lin Z, Gimelshein N, Antiga L, Desmaison A, Kopf A, Yang E, DeVito Z, Raison M, Tejani A, Chilamkurthy S, Steiner B, Fang L, Bai J and Chintala S 2019 *Advances in Neural Information Processing Systems 32* ed Wallach H, Larochelle H, Beygelzimer A, d'Alché-Buc F, Fox E and Garnett R (Curran Associates, Inc.) pp 8024–8035
- [30] Rueckauer B, Bybee C, Goettsche R, Singh Y, Mishra J and Wild A 2021 Nxtf: An api and compiler for deep spiking neural networks on intel loihi (*Preprint* 2101.04261)
- [31] Sign language mnist URL <https://www.kaggle.com/datamunge/sign-language-mnist>
- [32] Mavi A 2020 *arXiv preprint arXiv:2011.08927*
- [33] LeCun Y, Cortes C and Burges C 2010 *ATT Labs [Online]. Available: http://yann.lecun.com/exdb/mnist 2*
- [34] LeCun Y, Bottou L, Bengio Y and Haffner P 1998 *Proceedings of the IEEE* **86** 2278–2324
- [35] Krizhevsky A, Sutskever I and Hinton G E 2012 *Advances in neural information processing systems* **25** 1097–1105
- [36] Simonyan K and Zisserman A 2014 *arXiv preprint arXiv:1409.1556*
- [37] Abadi M, Agarwal A, Barham P, Brevdo E, Chen Z, Citro C, Corrado G S, Davis A, Dean J, Devin M, Ghemawat S, Goodfellow I, Harp A, Irving G, Isard M, Jia Y, Jozefowicz R, Kaiser L, Kudlur M, Levenberg J, Mané D, Monga R, Moore S, Murray D, Olah C, Schuster M, Shlens J, Steiner B, Sutskever I, Talwar K, Tucker P, Vanhoucke V, Vasudevan V, Viégas F, Vinyals O, Warden P, Wattenberg M, Wicke M, Yu Y and Zheng X 2015 TensorFlow: Large-scale machine learning on heterogeneous systems software available from tensorflow.org URL <https://www.tensorflow.org/>
- [38] URL <https://snntoolbox.readthedocs.io/en/latest/guide/citation.html>
- [39] Massa R, Marchisio A, Martina M and Shafique M 2020 *2020 International Joint Conference on Neural Networks (IJCNN)* (IEEE) pp 1–9
- [40] Buettner K and George A D 2021 *2021 IEEE Computer Society Annual Symposium on VLSI (ISVLSI)* (IEEE) pp 138–143
- [41] Intel 2019 Intel neural compute stick 2 URL <https://www.intel.com/content/www/us/en/developer/tools/neural-compute-stick/overview.html>
- [42] Amazon.2019.makerhawk um34 URL <https://www.amazon.com/MakerHawkBluetooth-Voltmeter-Multimeter-Resistance/dp/B07DK4GDSP>
- [43] Blouw P, Choo X, Hunsberger E and Eliasmith C 2019 *Proceedings of the 7th Annual Neuro-inspired Computational Elements Workshop* pp 1–8
- [44] URL [https://github.com/intel-nrc-ecosystem/models/tree/master/nxsdk\\_modules\\_ncl](https://github.com/intel-nrc-ecosystem/models/tree/master/nxsdk_modules_ncl)